

Heavy Ions in CMS

Thiago Rafael Fernandez Perez Tomei^{1,2,a} on behalf of the CMS Collaboration

¹*Institute for Theoretical Physics - Univ. Estadual Paulista, R. Dr. Bento Teobaldo Ferraz, 271, Barra Funda, CEP 01140-070 - São Paulo, SP, Brazil*

²*CERN – European Organization for Nuclear Research, CH-1211 Geneva 23, Switzerland*

Abstract. The capabilities of the CMS experiment allow to investigate various hard probes, as well as bulk particle production and collective phenomena, using the calorimetry, muon and tracking systems covering a large range in pseudorapidity. In this paper selected results of the CMS experiment from p-p and Pb-Pb collisions at $\sqrt{s_{NN}} = 2.76$ TeV are discussed. First results from the recent p-Pb Run at $\sqrt{s_{NN}} = 5.02$ TeV are also be presented.

1 Introduction

This paper reports on the latest results on heavy ions physics obtained by the CMS Collaboration. The Compact Muon Solenoid (CMS) is a high-energy physics experiment located at the Large Hadron Collider (LHC), CERN. The central feature of the CMS apparatus is a superconducting solenoid of 6 m internal diameter, providing a magnetic field of 3.8 T. Within the superconducting solenoid volume are a silicon pixel and strip tracker, a lead tungstate crystal electromagnetic calorimeter (ECAL), and a brass/scintillator hadron calorimeter (HCAL). Muons are measured in gas-ionization detectors embedded in the steel return yoke outside the solenoid. Extensive forward calorimetry complements the coverage provided by the barrel and endcap detectors; iron forward calorimeters (HF) with quartz fibers, read out by photomultipliers, extend the calorimeter coverage up to $|\eta| = 5.0$ and are used to classify the p-Pb and Pb-Pb collisions. A more detailed description can be found in Ref. [1]. All the detailed simulations of the interaction of the collision products with the CMS detector shown in these studies are made with GEANT4 [2].

2 Results of p-Pb Run in 2013

In the beginning of 2013, the LHC collider provided $1 \mu\text{b}^{-1}$ of proton-lead collisions at $\sqrt{s_{NN}} = 5.02$ TeV. Those data are used as an alternate environment, independent of Pb-Pb collisions, for the study of hot nuclear matter. We detail in this section the results of three measurements: two-particle correlations, dijet balance and charged hadron spectra.

^ae-mail: Thiago.Tomei@cern.ch

2.1 Two-particle correlations in p-Pb collisions

This analysis [3] focuses on long-range, near-side two-particle correlations. Events are collected online through usage of a track-based minimum bias trigger, where events are accepted if there is at least one track with $p_T > 400$ MeV in the pixel tracker. In the offline analysis, a coincidence of at least one HF calorimetric tower with $E > 3$ GeV on both the positive and negative sides of HF is required, in order to select hadronic collisions. Additionally, the presence of at least one reconstructed primary vertex with two tracks and a minimum fraction of good quality tracks is required in order to minimise beam-induced background. Those offline requirements are collectively called the "basic hadronic selection".

Tracks are considered for analysis only if they are "high purity" tracks, with $p_T > 100$ MeV and $|\eta| < 2.4$. The events are divided in four track multiplicity categories: $N_{trk} < 35$, $35-89$, $90-109$, > 110 tracks. The two-particle correlation function is given by:

$$\frac{1}{N_{trig}} \frac{d^2 N^{pair}}{d\Delta\eta d\Delta\phi} = B(0, 0) \times \frac{S(\Delta\eta, \Delta\phi)}{B(\Delta\eta, \Delta\phi)} \quad (1)$$

where $\Delta\eta$, $\Delta\phi$ are the differences in η and ϕ of the two particles. The signal distribution S is the per-trigger-particle yield for pairs from the same event, while B is the analogous distribution for pairs coming from different events, which are not correlated.

In Fig. 1, we can see the presence of a long-range structure in the azimuthal correlations for $2 < |\Delta\eta| < 4$, in the near-side region ($\Delta\phi \sim 0$). This result is qualitatively similar for that observed previously both in $\sqrt{s} = 7$ TeV p-p collisions and in nucleus-nucleus collisions. Figure 2 shows the associated yield for both 7 TeV p-p data and 5.02 TeV p-Pb data. The left plot shows the yield as a function of p_T for $N_{trk} > 110$, while the right plot shows the yield as function of multiplicity for $1 < p_T < 2$ GeV.

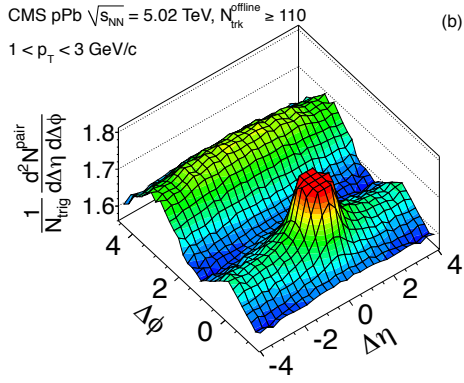


Figure 1. 2D two-particle correlation function for 5.02 TeV p-Pb collisions for pairs of charged particles with $1 < p_T < 3$ GeV for $N_{Trk} < 35$.

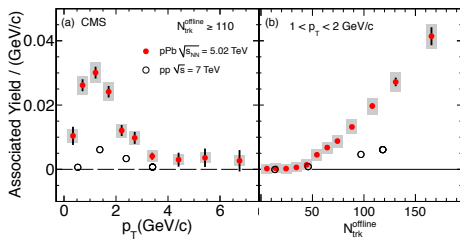


Figure 2. Associated yield for the near-side of the correlation function integrated over the region $2 < |\Delta\eta| < 4$ and $|\Delta\eta| < 1.2$ in 7 TeV pp collisions (open circles) and 5.02 TeV p-Pb collisions.

It can be seen that not only the absolute associated yield is larger in p-Pb collisions, but also that the correlations start to increase for $N_{Trk} \simeq 40$.

2.2 Dijet balance and pseudorapidity in p-Pb collisions

This analysis [4] studies dijet events in p-Pb collisions as a function of the forward calorimeter activity. The dijet momentum balance, the azimuthal angle correlations and the pseudo rapidity distributions are investigated. The events used in this analysis were selected using an inclusive single-jet trigger in the trigger, requiring a calorimeter-based jet with corrected transverse momentum $p_T > 100$ GeV. In addition to this jet data sample, a minimum bias event sample was selected by requiring at least one track with $p_T > 400$ MeV found in the pixel tracker system.

For the offline analysis, jets are reconstructed from Particle Flow [5] objects using the anti- k_T [6] algorithm with size parameter $R = 0.3$. To select a dijet topology, events are retained if the leading jet has $p_T > 120$ GeV, while the subleading jet has $p_T > 30$ GeV. Both jets should have $|\eta| < 3$, with an azimuthal distance $\Delta\phi > 2\pi/3$. No selection on the presence or absence of a third jet is performed. To further reduce noise, it is required that at either of the two jets has at least one track with $p_T > 4$ GeV. Basic collision requirements are also applied.

The selected minimum bias and dijet events are divided into forward activity categories using the raw trans-

verse energy measured by the HF detector. Figure 3 shows the HF transverse energy (E_T^{HF}) distribution for the selected dijet events and minimum bias events. It can be seen that the selection of high- p_T dijet event leads to a bias in the E_T^{HF} distribution towards higher values. The data are categorised in five E_T^{HF} bins: 0–20, 20–25, 25–30, 30–40 and 40–100 GeV, and compared both to PYTHIA [7] (pp collisions) and PYTHIA+HIJING [8] (p-Pb) simulations.

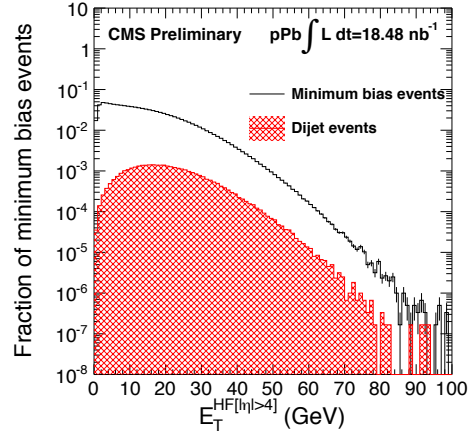


Figure 3. Probability distribution of the raw E_T measured by the HF detector in the pseudorapidity interval $|\eta| > 4$ for minimum bias collisions (black open histogram) and dijet events (red hatched histogram).

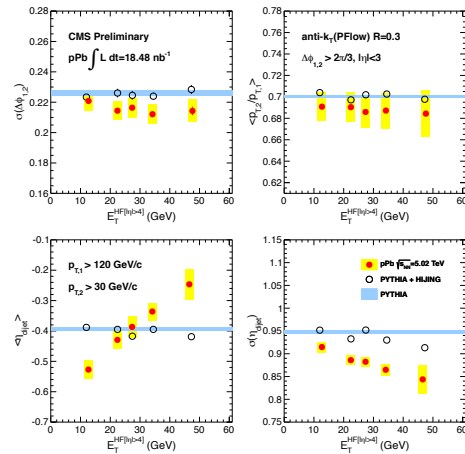


Figure 4. Summary of the dijet measurements as a function of E_T^{HF} . Top left: Fitted $\Delta\phi(1,2)$ width. Top right: Average ratio of dijet transverse momentum. Lower left: Mean of η dijet distribution. Lower right: Standard deviation of η dijet distribution.

From Fig. 4 it can be seen that, as a function of the forward calorimetric activity, the dijet pseudo rapidity distribution deviates from both the PYTHIA and the PYTHIA+HIJING predictions. No deviations on the dijet momentum balance and azimuthal correlation distributions are observed, however. These results show that the observed dijet asymmetry in Pb-Pb collisions is not originating from initial state effects, and the measurements can provide quantitative constraints on the nuclear parton distribution function.

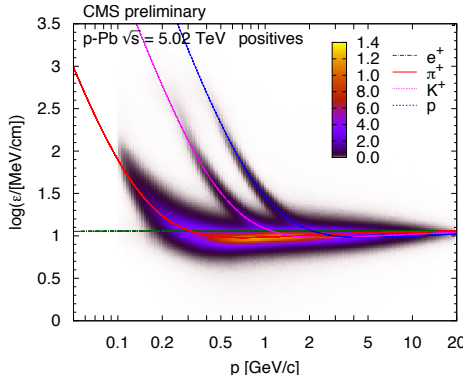


Figure 5. Distribution of $\log(\epsilon)$ as a function of total momentum p , for positive particles (ϵ is the most probable energy loss rate at a reference path-length $l_0 = 450\mu\text{m}$).

2.3 Charged hadron spectra in p-Pb collisions

This analysis [9] studies the spectra of charged hadrons in p-Pb collisions. The events used in this analysis were selected with the track-based minimum bias trigger. For the offline analysis only events with the presence of at least one tower with energy above 3 GeV in each of the HF calorimeters, were selected. Basic collision requirements were also applied. Only tracks with p_T in the range 0.1 to 1.7 GeV, $|\eta| < 1.0$ and passing quality requirements are considered. Tracks are then identified as from a given species of hadron (π , K, p) through their energy loss rate (ϵ) in the tracker material. The different ionisation curves can be seen in Fig. 5. It can be seen that particle identification capabilities are restricted to $p < 0.15$ GeV for electrons, $p < 1.20$ GeV for pions, $p < 1.05$ GeV for kaons, and $p < 1.70$ GeV for protons.

The efficiencies for event selection, tracking, and vertexing were evaluated by means of simulated event samples produced with the HIJING event generator. The independent species of hadrons yields were derived by direct counting (for low momentum tracks) and by template fits in $\log \epsilon$, in bins of p_T and η .

This study shows that the track average p_T increases rapidly with the mass of the hadron and with the event charged-particle multiplicity. In a comparison with the generators HIJING, AMPT [10] and EPOS (LHC) [11], it can be seen from Fig. 6 that all predict steeper p_T distributions and much smaller average p_T than found in data. Also, from Fig. 7 it can be seen that there are substantial deviation for the p/π ratios. This comparison can be used to constrain models of hadron production and contribute to the understanding of non-perturbative dynamics in hadronic collisions, through improvements of the models implemented in those generators.

3 Results of Pb-Pb Run in 2011

In 2011, the LHC collider provided $150 \mu\text{b}^{-1}$ of lead-lead collisions at $\sqrt{s_{NN}} = 2.76$ TeV. We detail in this section the results of two analyses: the measurement of the high-

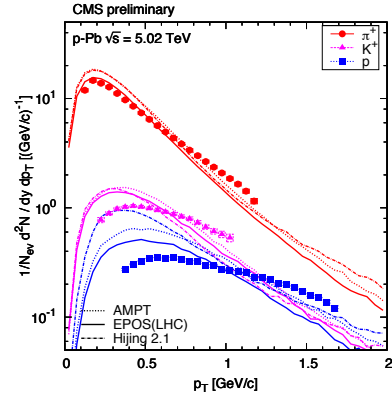


Figure 6. Transverse momentum distributions of identified charged hadrons (pions, kaons, protons) in the range $|\eta| < 1$,

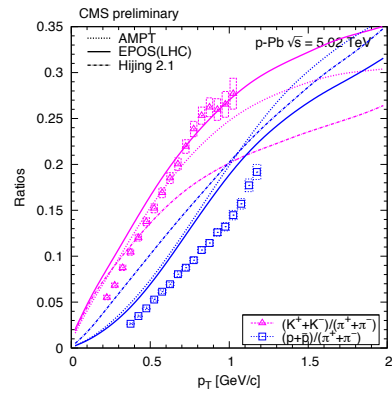


Figure 7. Ratios of particle yields as a function of transverse momentum.

p_T jet R_{AA} , and the study of very high p_T dihadron correlations.

3.1 High- p_T jet R_{AA} in Pb-Pb collisions

The goal of this analysis [12] is to study the jet nuclear modification factor R_{AA} in Pb-Pb collisions, searching for evidences of a change of the jet structure due to jet-medium interactions. Events are selected online through the presence of a calorimetric jet with $p_T > 80$ GeV. In the offline selection, jets are reconstructed from Particle Flow candidates, using the anti- k_T algorithm with a size parameter of $R=0.3$. Only events with jets with $p_T > 100$ GeV and $|\eta| < 2$ are considered. In addition, the ratio of the leading track in the jet to the total jet p_T is required to be larger than 1%. Basic collision requirements are also applied.

The collision centrality is determined from the deposition of transverse energy in HF, and it is divided into six bins: 0–5%, 5–10%, 10–30%, 30–50%, 50–70%, 70–90%. The experimentally determined centrality bins are correlated to the collision impact parameter using a Glauber model calculation [13]; the parameters related to centrality $\langle N_{part} \rangle$, $\langle N_{coll} \rangle$ and T_{AA} are shown in Table 1. The jet R_{AA} is then calculated as:

Table 1. The average number of participating nucleons $\langle N_{part} \rangle$, number of binary nucleon-nucleon collisions $\langle N_{coll} \rangle$, and nuclear overlap function $\langle T_{AA} \rangle$ for the centrality bins used in this analysis. The r.m.s. values give the spread over the centrality bins.

Centrality bin	$\langle N_{part} \rangle$	r.m.s.	$\langle N_{coll} \rangle$	r.m.s.	$\langle T_{AA} \rangle$ (mb ⁻¹)	r.m.s.
0–5%	381 ± 2	19.2	1660 ± 130	166	25.9 ± 1.06	2.60
5–10%	329 ± 3	22.5	1310 ± 110	168	20.5 ± 0.94	2.62
10–30%	224 ± 4	45.9	745 ± 67	240	11.6 ± 0.67	3.75
30–50%	108 ± 4	27.1	251 ± 28	101	3.92 ± 0.37	1.58
50–70%	42.0 ± 3.5	14.4	62.8 ± 9.4	33.4	0.98 ± 0.14	0.52
70–90%	11.4 ± 1.5	5.73	10.8 ± 2.0	7.29	0.17 ± 0.03	0.11

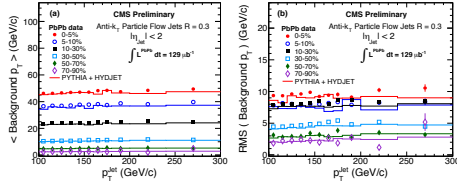


Figure 8. The mean and width of the underlying event background p_T that is subtracted from the jets for Pb-Pb data and simulated data.

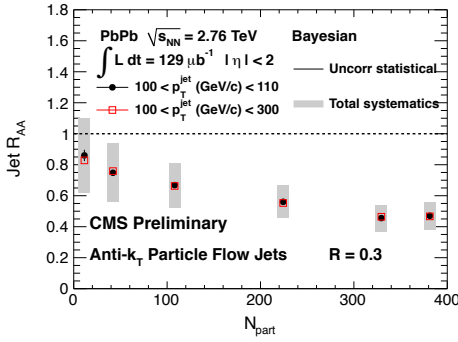


Figure 9. Bayesian unfolded jet R_{AA} for anti- k_T jets of $R=0.3$ as a function of N_{part} . Closed circles represent the jet R_{AA} for $100 < p_T < 110$ GeV, and open boxes the jet R_{AA} for $100 < p_T < 300$ GeV.

$$R_{AA} = \frac{dN_{jets}^{AA}/dp_T}{\langle N_{coll} \rangle dN_{jets}^{pp}/dp_T} = \frac{dN_{jets}^{AA}/dp_T}{\langle R_{AA} \rangle d\sigma_{jets}^{pp}/dp_T}. \quad (2)$$

The underlying event background is removed during jet reconstruction through the iterative “noise/pedestal subtraction” technique. Figure 8 shows the average background subtracted. However, due to the soft background prevalent in p-Pb collisions, further corrections are needed. In Fig. 9 the effects of a specific kind of unfolding (Bayesian) are shown, but the results are consistent within different methods of unfolding. The jet nuclear modification R_{AA} is measured to be approximately 0.5 for high centrality, while being consistent with 1 (meaning no suppression) for low centrality. Those results are shown to be independent of jet p_T and consistent with the usage of different cone sizes for the jet algorithm ($R = 0.2, 0.4$).

3.2 Very high p_T dihadron correlations

The final analysis we discuss here is the study of hadron correlations as function of the particle transverse momenta and collision centrality [14]. The goal of this analysis is to measure the I_{AA} modification factor, given by:

$$I_{AA}(p_T^{assoc}, p_T^{trig}) = \frac{Y_{jet_ind}^{AA}(p_T^{assoc}, p_T^{trig})}{Y_{jet_ind}^{pp}(p_T^{assoc}, p_T^{trig})}, \quad (3)$$

where $Y_{jet_ind}^{AA}(p_T^{assoc}, p_T^{trig})$ denotes the jet-induced yield in Pb-Pb (p-p) collisions. The differential per-trigger-particle associated yield is defined by:

$$\frac{1}{N_{trig}} \frac{d^2 N^{pair}}{d\Delta\eta d\Delta\phi} \quad (4)$$

which is integrated in (η, ϕ) to give the jet-induced yields defined above.

This analysis uses a single-track trigger with an additional jet requirement for events with total calorimetric $E_T < 100$ GeV. Events are further selected through the presence of calorimetric energy in the HF, plus basic hadronic collision selections. Tracks are considered in the p_T range 19.2–48 GeV (0.5–4 GeV) for trigger (associated) tracks. The centrality of the Pb-Pb reaction is determined by taking fractions of the total hadronic inelastic cross section, according to percentiles of the distribution of the total energy deposited in the HF calorimeters. The centrality bins used in this analysis are 0–10%, 10–20%, 20–30%, 30–40%, 40–50%, and 50–60%.

To obtain a clean measurement of I_{AA} , we subtract the contribution from the single-particle azimuthal anisotropies. The subtracted term is given by:

$$a_0 \left(1 + 2 \sum_n v_n(p_T^{trig}) v_n(p_T^{assoc}) \cos(n\Delta\phi) \right), \quad (5)$$

where the coefficients $v_n(p_T^{trig})$ and $v_n(p_T^{assoc})$ are the single-particle azimuthal anisotropy harmonics for the trigger and associated particles, respectively. The a_0 parameter is extracted by the Zero-Yield-At-Minimum procedure [15], which assumes that, for the jet-like correlations, the correlated yield drops to zero in a certain $\Delta\phi$ around $\pi/2$. The $v_n(p_T)$ values are determined using the event-plane method.

Our measurements show that, at the away side ($\Delta\phi \sim \pi$), for very central (0-10%) Pb-Pb collisions, there is a large enhancement of I_{AA} , by a factor of around 3–4, at low p_T^{assoc} ; for high p_T^{assoc} there is a suppression of around 50% instead. This suggests that the energy loss of the high- p_T partons in the medium is converted to low p_T particles. On the near side ($\Delta\phi \sim 0$), instead, there’s a significantly smaller difference between the p-p and Pb-Pb collision. That is consistent with a minimal energy loss of the higher- p_T^{trig} particle predominantly coming from the surface of the medium.

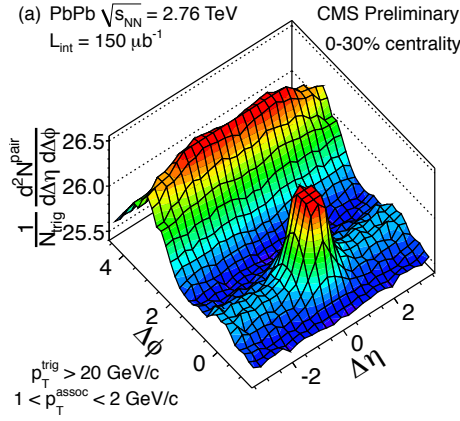


Figure 10. The per-trigger-particle associated yield of charged particles in two-dimension as a function of $|\Delta\eta|$ and $|\Delta\phi|$ for $p_T^{\text{trig}} > 20$ GeV/c and $1 < p_T^{\text{assoc}} < 3$ GeV/c from the 0–30% centrality range of Pb-Pb collisions

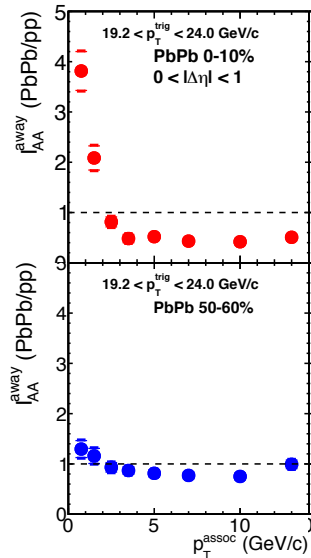


Figure 11. Away-side I_{AA} values derived from v_n -subtraction method at $|\Delta\eta| < 1$, for for 0–10% centrality (top) 50–60% centrality. (bottom)

4 Conclusions

The first CMS results of the p-Pb run at $\sqrt{s_{NN}} = 5.02$ TeV are starting to become available, while many analyses of the 2011 Pb-Pb run are in the finishing stages. The results shown in the analyses discussed here can already put constraints in different models for description of hot nuclear matter. We foresee that CMS will continue to deliver quality heavy-ion results in the coming years.

5 Acknowledgements

We congratulate our colleagues in the CERN accelerator departments for the excellent performance of the LHC and thank the technical and administrative staffs at CERN and at other CMS

institutes for their contributions to the success of the CMS effort. We gratefully acknowledge the computing centres and personnel of the Worldwide LHC Computing Grid for delivering the computing infrastructure essential to our analyses. Finally, we acknowledge the enduring support for the construction and operation of the LHC and the CMS detector provided by the following funding agencies: BMWF and FWF (Austria); FNRS and FWO (Belgium); CNPq, CAPES, FAPERJ, and FAPESP (Brazil); MES (Bulgaria); CERN; CAS, MoST, and NSFC (China); COLCIENCIAS (Colombia); MSES (Croatia); RPF (Cyprus); MoER, SF0690030s09 and ERDF (Estonia); Academy of Finland, MEC, and HIP (Finland); CEA and CNRS/IN2P3 (France); BMBF, DFG, and HGF (Germany); GSRT (Greece); OTKA and NKTH (Hungary); DAE and DST (India); IPM (Iran); SFI (Ireland); INFN (Italy); NRF and WCU (Republic of Korea); LAS (Lithuania); CINVESTAV, CONACYT, SEP, and UASLP-FAI (Mexico); MBIE (New Zealand); PAEC (Pakistan); MSHE and NSC (Poland); FCT (Portugal); JINR (Dubna); MON, RosAtom, RAS and RFBR (Russia); MESTD (Serbia); SEIDI and CPAN (Spain); Swiss Funding Agencies (Switzerland); NSC (Taipei); ThEPCenter, IPST, STAR and NSTDA (Thailand); TUBITAK and TAEK (Turkey); NASU (Ukraine); STFC (United Kingdom); DOE and NSF (USA).

References

- [1] S. Chatrchyan et al. (CMS), *JINST* **3**, S08004 (2008)
- [2] S. Agostinelli et al. (GEANT4), *Nucl. Instrum. Meth.* **A506**, 250 (2003)
- [3] S. Chatrchyan et al. (CMS Collaboration), *Phys.Lett.* **B718**, 795 (2013), 1210.5482
- [4] Tech. Rep. CMS-PAS-HIN-13-001, CERN, Geneva (2013)
- [5] CMS Collaboration, CMS Physics Analysis Summary **PFT-10-002** (2010)
- [6] M. Cacciari, G.P. Salam, G. Soyez, *JHEP* **0804**, 063 (2008), 0802.1189
- [7] T. Sjostrand, P. Edénb, C. Friberg, L. Lönnblada, G. Miu, S. Mrennac, E. Norrbin., *Comput. Phys. Commun.* **135**, 238 (2001)
- [8] M. Gyulassy, X.N. Wang, *Comput.Phys.Commun.* **83**, 307 (1994), nucl-th/9502021
- [9] Tech. Rep. CMS-PAS-HIN-12-016, CERN, Geneva (2013)
- [10] Z. Lin, *Indian J.Phys.* **85**, 837 (2011)
- [11] S. Porteboeuf, T. Pierog, K. Werner (2010), 1006.2967
- [12] Tech. Rep. CMS-PAS-HIN-12-004, CERN, Geneva (2012)
- [13] M.L. Miller, K. Reygers, S.J. Sanders, P. Steinberg, *Ann.Rev.Nucl.Part.Sci.* **57**, 205 (2007), nucl-ex/0701025
- [14] Tech. Rep. CMS-PAS-HIN-12-010, CERN, Geneva (2012)
- [15] N.N. Ajitanand, J.M. Alexander, P. Chung, W.G. Holzmann, M. Issah, R.A. Lacey, A. Shevel, A. Taranenko, P. Danielewicz, *Phys. Rev. C* **72**, 011902 (2005)